Optical-Fiber Gravitational Wave Detector: Dynamical 3-Space Turbulence Detected

Reginald T. Cahill

School of Chemistry, Physics and Earth Sciences, Flinders University, Adelaide 5001, Australia
E-mail: Reg.Cahill@flinders.edu.au

Preliminary results from an optical-fiber gravitational wave interferometric detector are reported. The detector is very small, cheap and simple to build and operate. It is assembled from readily available opto-electronic components. A parts list is given. The detector can operate in two modes: one in which only instrument noise is detected, and data from a 24 hour period is reported for this mode, and in a 2nd mode in which the gravitational waves are detected as well, and data from a 24 hour period is analysed. Comparison shows that the instrument has a high S/N ratio. The frequency spectrum of the gravitational waves shows a pink noise spectrum, from 0 to 0.1 Hz.

1 Introduction

Preliminary results from an optical-fiber gravitational wave interferometric detector are reported. The detector is very small, cheap and simple to build and operate, and is shown in Fig. 1. It is assembled from readily available opto-electronic components, and is suitable for amateur and physics undergraduate laboratories. A parts list is given. The detector can operate in two modes: one in which only instrumental noise is detected, and the 2nd in which the gravitational waves are detected as well. Comparison shows that the instrument has a high S/N ratio. The frequency spectrum of the gravitational waves shows a pink noise spectrum, from essentially 0 to 0.1 Hz. The interferometer is 2nd order in v/c and is analogous to a Michelson interferometer. Michelson interferometers in vacuum mode cannot detect the light-speed anisotropy effect or the gravitational waves manifesting as light-speed anisotropy fluctuations. The design and operation as well as preliminary data analysis are reported here so that duplicate detectors may be constructed to study correlations over various distances. The source of the gravitational waves is unknown, but a 3D multi-interferometer detector will soon be able to detect directional characteristics of the waves.

2 Light speed anisotropy

In 2002 it was reported [1, 2] that light-speed anisotropy had been detected repeatedly since the Michelson-Morley experiment of 1887 [3]. Contrary to popular orthodoxy they reported a light-speed anisotropy up to 8 km/s based on their analysis of their observed fringe shifts. The Michelson-Morley experiment was everything except *null*. The deduced speed was based on Michelson's Newtonian-physics calibration for the interferometer. In 2002 the necessary special relativity effects and the effects of the air present in the light paths were first taken into account in calibrating the interferometer. This reanalysis showed that the actual observed fringe shifts
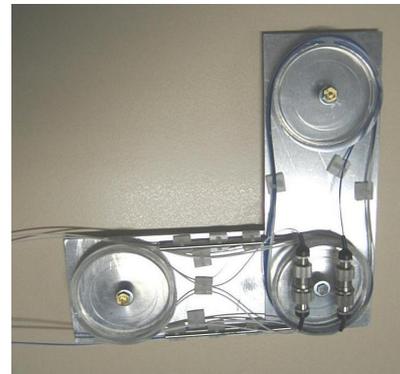

Fig. 1: Photograph of the detector showing the fibers forming the two orthogonal arms. See Fig. 2 for the schematic layout. The beam splitter and joiner are the two small stainless steel cylindrical tubes. The two FC to FC mating sleeves are physically adjacent, and the fibers can be re-connected to change from Mode A (Active detector — gravitational wave and device noise detection) to Mode B (Background — device noise measurements only). The overall dimensions are 160mm × 160mm. The 2×2 splitter and joiner each have two input and two output fibers, with one not used.

corresponded to a very large light-speed anisotropy, being in excess of 1 part in 1000 of $c = 300,000$ km/s. The existence of this light-speed anisotropy is not in conflict with the successes of Special Relativity, although it is in conflict with Einstein's postulate that the speed of light is invariant. This large light-speed anisotropy had gone unnoticed throughout the twentieth century, although we now know that it was detected in seven experiments, ranging from five 2nd order in v/c gas-mode Michelson-interferometer experiments [3–7] to two 1st order in v/c one-way RF coaxial cable travel-speed measurements using atomic clocks [8, 9]. In 2006 another RF travel time coaxial cable experiment was performed [10]. All eight light-speed anisotropy experiments agree [11, 12]. Remarkably five of these experiments [3, 4, 8, 9, 10] reveal pronounced *gravitational wave* effects, where the meaning of this term is explained below. In particular detailed analysis of
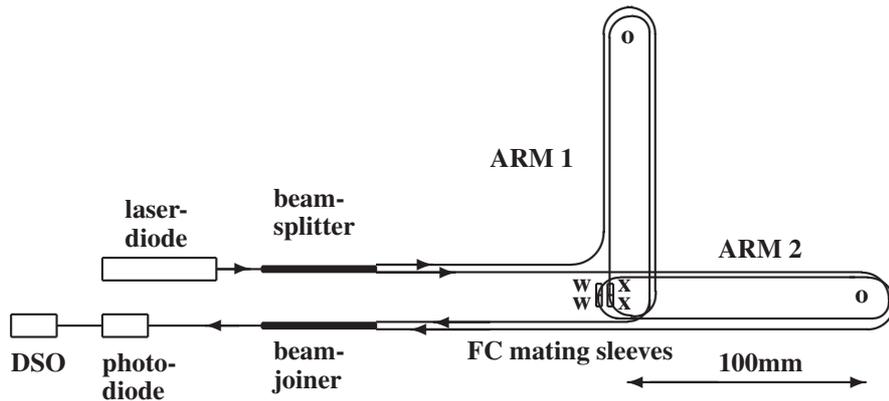
Fig. 2: Schematic layout of the interferometric optical-fiber light-speed anisotropy/gravitational wave detector (in Mode **A**). Actual detector is shown in Fig.1, with ARM2 located to the left, so as to reduce lengths of fiber feeds and overall size. Coherent 650 nm light from the laser diode is split into two 1m length single-mode polarisation preserving fibers by the beam splitter. The two fibers take different directions, ARM1 and ARM2, after which the light is recombined in the beam joiner, which also has 1m length fibers, in which the phase differences lead to interference effects that are indicated by the outgoing light intensity, which is measured in the photodiode, and then recorded in the Digital Storage Oscilloscope (DSO). In Mode **A** the optical fibers are joined $x - x$ and $w - w$ at the FC to FC mating sleeves, as shown. In the actual layout the fibers make four loops in each arm, and the length of one straight section is 100 mm, which is the center to center spacing of the plastic turners, having diameter = 52 mm, see Fig. 1. The two FC to FC mating sleeves are physically adjacent and by re-connecting the fibers as $x - w$ and $w - x$ the light paths can be made symmetrical wrt the arms, giving Mode **B**, which only responds to device noise — the **B**ackground mode. In Mode **A** the detector is **A**ctive, and responds to both flowing 3-space and device noise. The relative travel times, and hence the output light intensity, are affected by the fluctuating speed and direction of the flowing 3-space, by affecting differentially the speed of the light, and hence the net phase difference between the two arms.

the Michelson-Morley fringe shift data shows that they not only detected a large light-speed anisotropy, but that their data also reveals large wave effects [12]. The reason why their interferometer could detect these phenomena was that the light paths passed through air; if a Michelson interferometer is operated in vacuum then changes in the geometric light-path lengths exactly cancel the Fitzgerald-Lorentz arm-length contraction effects. This cancellation is incomplete when a gas is present in the light paths. So modern vacuum Michelson interferometers are incapable of detecting the large light-speed anisotropy or the large gravitational waves. Here we detail the construction of a simple optical-fiber light-speed anisotropy detector, with the main aim being to record and characterise the gravitational waves. These waves reveal a fundamental aspect to reality that is absent in the prevailing models of reality.

3 Dynamical 3-Space and gravitational waves

The light-speed anisotropy experiments reveal that a dynamical 3-space exists, with the speed of light being c only wrt to this space: observers in motion "through" this 3-space detect that the speed of light is in general different from c, and is different in different directions. The notion of a dynamical 3-space is reviewed in [11, 12]. The dynamical equations for this 3-space are now known and involve a velocity field $\mathbf{v}(\mathbf{r}, t)$, but where only relative velocities are observable. The coordinates $\mathbf{r}$ are relative to a non-physical mathematical embedding space. These dynamical equations involve Newton's gravitational constant G and the fine structure constant α. The discovery of this dynamical 3-space then required a generalisation of the Maxwell, Schrödinger and Dirac equations. In particular these equations showed that the phenomenon of gravity is a wave refraction effect, for both EM waves and quantum matter waves [12, 13]. This new physics has been confirmed by explaining the origin of gravity, including the Equivalence Principle, gravitational light bending and lensing, bore hole g anomalies, spiral galaxy rotation anomalies (so doing away with the need for dark matter), black hole mass systematics, and also giving an excellent parameter-free fit to the supernovae and gamma-ray burst Hubble expansion data [14] (so doing away with the need for dark energy). It also predicts a novel spin precession effect in the GPB satellite gyroscope experiment [15]. This physics gives an explanation for the successes of the Special Relativity formalism, and the geodesic formalism of General Relativity. The wave effects already detected correspond to fluctuations in the 3-space velocity field $\mathbf{v}(\mathbf{r}, t)$, so they are really 3-space turbulence or wave effects. However they are better known, if somewhat inappropriately as "gravitational waves" or "ripples" in "spacetime". Because the 3-space dynamics gives a deeper understanding of the spacetime formalism, we now know that the metric of the induced spacetime, merely a mathematical construct having no ontological significance, is related to $\mathbf{v}(\mathbf{r}, t)$ according to [11, 12]

$$ds^2 = dt^2 - \frac{\left(d\mathbf{r} - \mathbf{v}(\mathbf{r}, t)dt \right)^2}{c^2} = g_{\mu\nu} \, dx^\mu dx^\nu. \quad (1)$$

The gravitational acceleration of matter, and of the structural patterns characterising the 3-space, is given by [12, 13]

$$\mathbf{g} = \frac{\partial \mathbf{v}}{\partial t} + (\mathbf{v} \cdot \nabla)\mathbf{v} \qquad (2)$$

and so fluctuations in $\mathbf{v}(\mathbf{r}, t)$ may or may not manifest as a gravitational force. The general characteristics of $\mathbf{v}(\mathbf{r}, t)$ are now known following the detailed analysis of the eight experiments noted above, namely its average speed, over an hour or so, of some 420 ± 30 km/s, and direction RA $= 5.5 \pm 2^{\mathrm{hr}}$, Dec $= 70 \pm 10° $S, together with large wave/turbulence effects. The magnitude of this turbulence depends on the timing resolution of each particular experiment, and here we report that the speed fluctuations are very large, as also seen in [10] Here we employ a new detector design that enables a detailed study of $\mathbf{v}(\mathbf{r}, t)$, and with small timing resolutions. A key experimental test of the various detections of $\mathbf{v}(\mathbf{r}, t)$ is that the data shows that the time-averaged $\mathbf{v}(\mathbf{r}, t)$ has a direction that has a specific Right Ascension and Declination as given above, i.e. the time for say a maximum averaged speed depends on the local sidereal time, and so varies considerably throughout the year, as do the directions to all astronomical processes/objects. This sidereal effect constitutes an absolute proof that the direction of $\mathbf{v}(\mathbf{r}, t)$ and the accompanying wave effects are real "astronomical" phenomena, as there is no known earth-based effect that can emulate the sidereal effect.

4 Gravitational wave detector

To measure $\mathbf{v}(\mathbf{r}, t)$ has been difficult until now. The early experiments used gas-mode Michelson interferometers, which involved the visual observation of small fringe shifts as the relatively large devices were rotated. The RF coaxial cable experiments had the advantage of permitting electronic recording of the RF travel times, over 500 m [8] and 1.5 km [9], by means of two or more atomic clocks, although the experiment reported in [10] used a novel technique that enable the coaxial cable length to be reduced to laboratory size. The new detector design herein has the advantage of electronic recording as well as high precision because the travel time differences in the two orthogonal fibers employ light interference effects, with the interference effects taking place in an optical beam-joiner, and so no optical projection problems arise. The device is very small, very cheap and easily assembled from readily available opto-electronic components. The schematic layout of the detector is given in Fig. 2, with a detailed description in the figure caption. The detector relies on the phenomenon where the 3-space velocity $\mathbf{v}(\mathbf{r}, t)$ affects differently the light travel times in the optical fibers, depending on the projection of $\mathbf{v}(\mathbf{r}, t)$ along the fiber directions. The differences in the light travel times are measured by means of the interference effects in the beam joiner. However at present the calibration constant k of the device is not yet known, so it is not yet known what speed corresponds to the measured

Parts	Thorlabs http://www.thorlabs.com/
1x Si Photodiode Detector/ Amplifier/Power Supply	PDA36A or PDA36A-EC select for local AC voltage
1xFiber Adaptor for above	SM1FC
1xFC Fiber Collimation Pkg	F230FC-B
1xLens Mounting Adaptor	AD1109F
2xFC to FC Mating Sleeves	ADAFC1
2x 2x2 Beam Splitters	FC632-50B-FC
Fiber Supports	PFS02
	Midwest Laser Products http://www.midwest-laser.com/
650nm Laser Diode Module	VM65003
LDM Power Supply/3VDC	**Local Supplier or Batteries**
BNC 50Ω coaxial cable	**Local Supplier**
	PoLabs
PoScope USB DSO	http://www.poscope.com/

Table 1: List of parts and possible suppliers for the detector. The FC Collimation Package and Lens Mounting Adaptor together permit the coupling of the Laser Diode Module to the optical fiber connector. This requires unscrewing the lens from the Laser Diode Module and screwing the diode into above and making judicious adjustment to maximise light coupling. The coaxial cable is required to connect the photodiode output to the DSO. Availability of a PC to host the USB DSO is assumed. The complete detector will cost $\approx$ \$1100 US dollars.

time difference Δt, although comparison with the earlier experiments gives a guide. In general we expect

$$\Delta t = k^2 \frac{L v_P^2}{c^3} \cos\big(2(\theta - \psi)\big) \qquad (3)$$

where k is the instrument calibration constant. For gas-mode Michelson interferometers k is known to be given by $k^2 \approx$ $\approx n^2 - 1$, where n is the refractive index of the gas. Here $L = 4 \times 100$ mm is the effective arm length, achieved by having four loops of the fibers in each arm, and v_P is the projection of $\mathbf{v}(\mathbf{r}, t)$ onto the plane of the detector. The angle θ is that of the arm relative to the local meridian, while ψ is the angle of the projected velocity, also relative to the local meridian. A photograph of the prototype detector is shown in Figure 1.

A key component is the light source, which can be the laser diode listed in the Table of parts. This has a particularly long coherence length, unlike most cheap laser diodes, although the data reported herein used a more expensive He-Ne laser. The other key components are the fiber beam splitter/joiner, which split the light into the fibers for each arm, and recombine the light for phase difference measurements by means of the fiber-joiner and photodiode detector and amplifier. A key feature of this design is that the detector can oper-
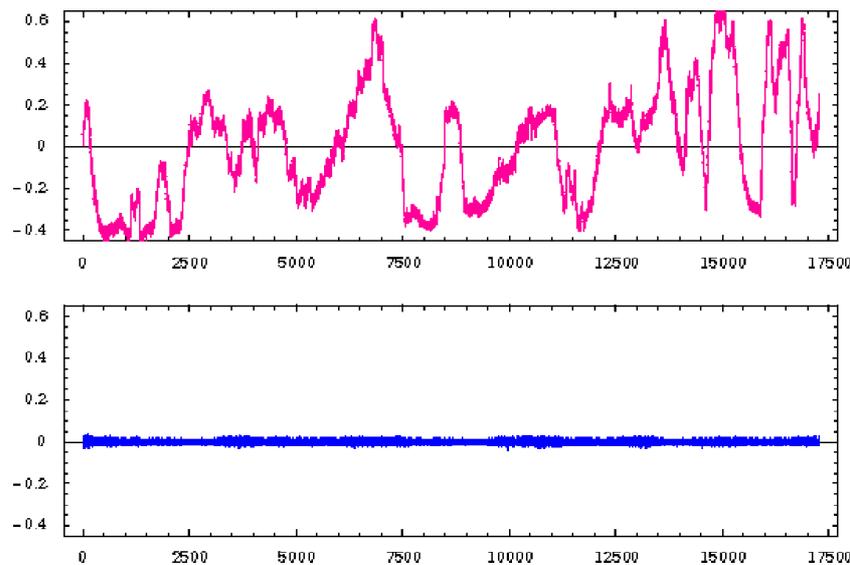
Fig. 3: Photodiode voltages over a 24 hour period with data recording every 5 s, with the detector arms orientated in a NS-EW direction and horizontal. Upper plot (red) is for detector in Mode A, i.e responding to 3-space dynamics and instrument noise, while lower plot (blue) is for Mode B in which detector only responds to instrumental noise, and demonstrates the high S/N ratio of the detector. The lower plot is dominated by higher frequency noise, as seen in the frequency spectrum in Fig. 5. A selection of the above data over a 1 hour time interval, from time steps 4900 to 5620, is shown in Fig. 4 indicating details of the 3-space wave forms.

ate in two different modes. In Mode **A** the detector is **A**ctive, and responds to both flowing 3-space and device noise. Because the two fiber coupler (FC) mating sleeves are physically adjacent a re-connection of the fibers at the two mating sleeves makes the light paths symmetrical wrt the arms, and then the detector only responds to device noise; this is the **B**ackground mode. The data stream may be mostly cheaply recorded by a PoScope USB Digital Storage Oscilloscope (DSO) that runs on a PC.

The interferometer operates by detecting the travel time difference between the two arms as given by (3). The cycle-averaged light intensity emerging from the beam joiner is given by

$$I(t) \;\propto\; \left| \mathbf{E}_1\, e^{i\omega t} + \mathbf{E}_2\, e^{i\omega(t+\tau+\Delta t)} \right|^2$$
$$= |\mathbf{E}|^2 \cos\left(\frac{\omega(\tau+\Delta t)}{2} \right)^2 \approx a + b\Delta t. \qquad (4)$$

Here $\mathbf{E}_i$ are the electric field amplitudes and have the same value as the fiber splitter/joiner are 50%-50% types, and having the same direction because polarisation preserving fibers are used, ω is the light angular frequency and τ is a travel time difference caused by the light travel times not being identical, even when $\Delta t = 0$, mainly because the various splitter/joiner fibers will not be identical in length. The last expression follows because Δt is small, and so the detector operates in a linear regime, in general, unless τ has a value equal to modulo(T), where T is the light period. The main temperature effect in the detector is that τ will be temperature dependent. The photodiode detector output voltage $V(t)$

is proportional to $I(t)$, and so finally linearly related to Δt. The detector calibration constants a and b depend on k and τ, and are unknown at present, and indeed τ will be instrument dependent. The results reported herein show that the value of the calibration constant b is not given by using the effective refractive index of the optical fiber in (3), with b being much smaller than that calculation would suggest. This is in fact very fortunate as otherwise the data would be affected by the need to use the cosine form in (4), and thus would suffer from modulo effects. It is possible to determine the voltages for which (4) is in the non-linear regime by spot heating a segment of one fiber by touching with a finger, as this produces many full fringe shifts.

By having three mutually orthogonal optical-fiber interferometers it is possible to deduce the vectorial direction of $\mathbf{v}(\mathbf{r}, t)$, and so determine, in particular, if the pulses have any particular direction, and so a particular source. The simplicity of this device means that an international network of detectors may be easily set up, primarily to test for correlations in the waveforms.

5 Data analysis

Photodiode voltage readings from the detector in Mode **A** on July 11, 2007, from approximately 12:30pm local time for 24 hours, and in Mode **B** June 24 from 4pm local time for 24 hours, are shown in Fig. 3, with an arbitrary zero. The photodiode output voltages were recorded every 5 s. Most importantly the data are very different, showing that only in Mode **A** are gravitational waves detected, and with a high S/N
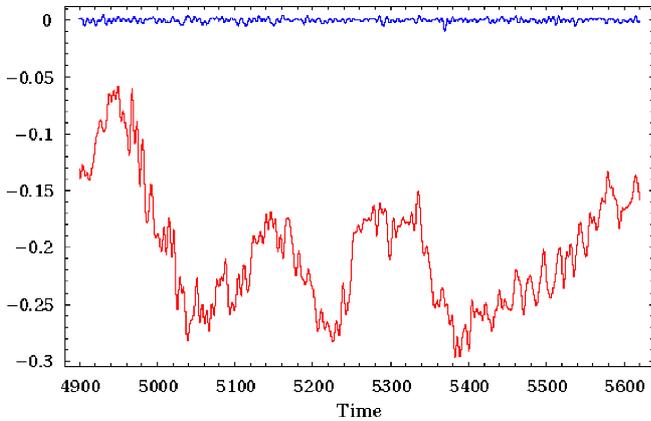
Fig. 4: Lower plot (red) shows the time series data over a 1 hour period, from time steps 4900 to 5620 in Fig. 3, showing the wave forms present in Fig. 3 in greater detail. Similar complex wave forms were seen in [10]. These plots were reconstructed from the FT after band passing the frequencies (1–3000)$\times 1.16 \times 10^{-5}$Hz=(0.000116–0.034) Hz to reduce the instrument noise component, which is very small as shown in upper plot (blue).
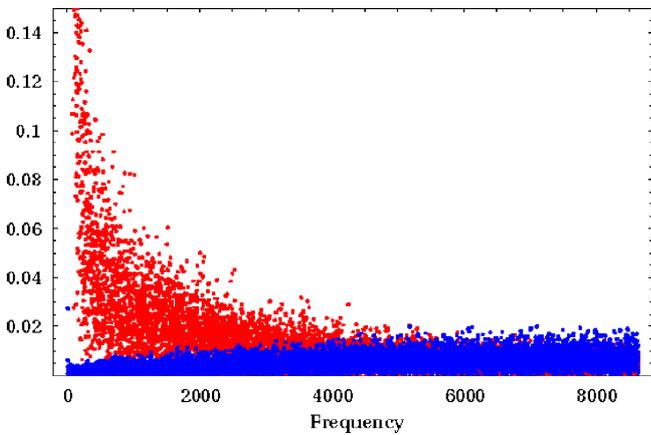

Fig. 5: Two plots of $|\tilde{V}_s|$ from Fast Fourier Transforms of the photodiode detector voltage V_r at 5 second intervals for 24 fours. Frequency step corresponds to 1.157×10^{-5}Hz. Upper frequency spectrum (red) is for detector in Mode A, i.e responding to 3-space dynamics and instrument noise, while lower spectrum (blue) is for Mode B in which detector only responds to instrumental noise. We see that the signal in Mode A is very different from that Mode B operation, showing that the S/N ratio for the detector is very high. The instrumental noise has a mild "blue" noise spectrum, with a small increase at higher frequencies, while the 3-space turbulence has a distinctive "pink" noise spectrum.
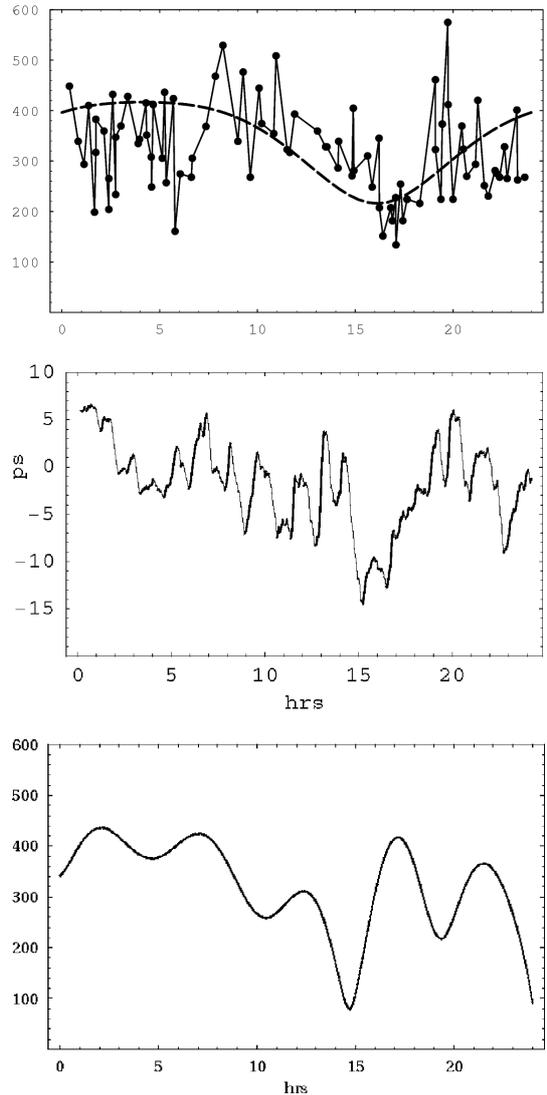

Fig. 6: *Top*: Absolute projected speeds v_P in the Miller experiment plotted against sidereal time in hours for a composite day collected over a number of days in September 1925. Maximum projected speed is 417 km/s. The data shows considerable fluctuations. The dashed curve shows the non-fluctuating variation expected over one day as the Earth rotates, causing the projection onto the plane of the interferometer of the velocity of the average direction of the 3-space flow to change. *Middle*: Data from the Cahill experiment [10] for one sidereal day on approximately August 23, 2006. We see similar variation with sidereal time, and also similar wave structure. This data has been averaged over a running 1hr time interval to more closely match the time resolution of the Miller experiment. These fluctuations are real wave phenomena of the 3-space. *Bottom*: Data from the optical-fiber experiment herein with only low frequencies included to simulate the time averaging in the other two experiments. Comparison permits an approximate calibration for the optical fiber detector, as indicated by the speed in km/s.

ratio. A 1 hour time segment of that data is shown in Fig. 4. In that plot the higher frequencies have been filtered out from both data time series, showing the exceptional S/N ratio that can be achieved.

In Fig. 5 the Fourier Transfoms of the two data time series are shown, again revealing the very different characteristics of the data from the two operating modes. The instrumental noise has a mild "blue" noise spectrum, with a small increase at higher frequencies, while the 3-space turbulence has a distinctive "pink" noise spectrum, and ranging essentially from 0 to 0.1 Hz. The FT is defined by

$$\widetilde{V}_s = \frac{1}{\sqrt{n}} \sum_{r=1}^{n} V_r e^{2\pi i (r-1)(s-1)/n} \tag{5}$$

where $n = 17280$ corresponds to a 5 s timing interval over 24 hours.

By removing all but the FT amplitudes 1–10, and then inverse Fourier Transforming we obtain the slow changes occurring over 24 hours. The resulting data has been presented in terms of possible values for the projected speed v_P in (3), and is shown in Fig. 6 and plotted against sidereal time, after adjusting the unknown calibration constants to give a form resembling the Miller and coaxial cable experimental results so as to give some indication of the calibration of the detector. The experiment was run in an unoccupied office in which temperatures varied by some $10°C$ over the 24 hour periods. In future temperature control will be introduced.

6 Conclusions

As reviewed in [11, 12] gravitational waves, that is, fluctuations or turbulence in the dynamical 3-space, have been detected since the 1887 Michelson-Morley experiment, although this all went unrealised until recently. As the timing resolution improved over the century, from initially one hour to seconds now, the characteristics of the turbulence of the dynamical 3-space have become more apparent, and that at smaller timing resolutions the turbulence is seen to be very large. As shown herein this wave/pulse phenomenon is very easy to detect, and opens up a whole new window on the universe. The detector reported here took measurements every 5 s, but can be run at millisecond acquisition rates. A 3D version of the detector with three orthogonal optical-fiber interferometers will soon become operational. This will permit the determination of the directional characteristics of the 3-space pulses.

That the average 3-space flow will affect the gyroscope precessions in the GP-B satellite experiment through vorticity effects was reported in [15]. The fluctuations are also predicted to be detectable in that experiment as noted in [16]. However the much larger fluctuations detected in [10] and herein imply that these effects will be much large than reported in [16] where the time averaged waves from the De-

Witte experiment [9] were used; essentially the gyro precessions will appear to have a large stochasticity.

References

1. Cahill R.T. and Kitto K. Michelson-Morley experiments revisited. *Apeiron*, 2003, v. 10 (2),104–117.

2. Cahill R.T. The Michelson and Morley 1887 experiment and the discovery of absolute motion. *Progress in Physics*, 2005, v. 3, 25–29.

3. Michelson A. A. and Morley E. W. *Philos. Mag.*, 1887, S. 5, 24, No. 151, 449–463.

4. Miller D. C. *Rev. Mod. Phys.*, 1933, v. 5, 203–242.

5. Illingworth K. K. *Phys. Rev.*, 1927, v. 3, 692–696.

6. Joos G. *Ann. d. Physik*, 1930, v. 7, 385.

7. Jaseja T. S. *et al. Phys. Rev. A*, 1964, v. 133, 1221.

8. Torr D. G. and Kolen P. In: *Precision Measurements and Fundamental Constants*, Taylor, B. N. and Phillips, W. D. eds., Natl. Bur. Stand. (U.S.), Spec. Publ., 1984, v. 617, 675.

9. Cahill R. T. The Roland DeWitte 1991 experiment. *Progress in Physics*, 2006, v. 3, 60–65.

10. Cahill R. T. A new light-speed anisotropy experiment: absolute motion and gravitational waves detected. *Progress in Physics*, 2006, v. 4, 73–92.

11. Cahill R. T. Process physics: from information theory to quantum space and matter. Nova Science Pub., New York, 2005.

12. Cahill R. T. Dynamical 3-space: a review. arXiv: 0705.4146.

13. Cahill R. T. Dynamical fractal 3-space and the generalised Schrödinger equation: equivalence principle and vorticity effects. *Progress in Physics*, 2006, v. 1, 27–34.

14. Cahill R. T. Dynamical 3-space: supernovae and the Hubble expansion — the older Universe without Dark Energy. *Progress in Physics*, 2007, v. 4, 9–12.

15. Cahill R. T. Novel Gravity Probe B frame-dragging effect. *Progress in Physics*, 2005, v. 3, 30–33.

16. Cahill R. T. Novel Gravity Probe B gravitational wave detection. arXiv: physics/0407133.